Applied Catalysis B: Environmental 123–124 (2012) 27–35

Contents lists available at SciVerse ScienceDirect

Applied Catalysis B: Environmental

journal homepage: www.elsevier.com/locate/apcatb

Cu-modified cryptomelane oxide as active catalyst for CO oxidation reactions

Willinton Y. Hernández[a,*], Miguel A. Centeno[a], Svetlana Ivanova[a], Pierre Eloy[b], Eric M. Gaigneaux[b], José A. Odriozola[a]

[a] Departamento de Química Inorgánica e Instituto de Ciencia de Materiales de Sevilla, Centro Mixto Universidad de Sevilla-CSIC, Avda. Américo Vespuccio 49, 41092 Seville, Spain
[b] Université catholique de Louvain, Institute of Condensed Matter and Nanosciences, Division Molecules, Solids and Reactivity, Croix du Sud 2/17, B-1348 Louvain-la-Neuve, Belgium

ARTICLE INFO

Article history:
Received 1 March 2012
Received in revised form 17 April 2012
Accepted 19 April 2012
Available online 25 April 2012

Keywords:
CO oxidation
Manganese oxides
Octahedral molecular sieve (OMS)
Cu-modified cryptomelane

ABSTRACT

Manganese oxide octahedral molecular sieves (cryptomelane structure) were synthesized by a solvent-free method and tested in the total oxidation of CO (TOX), and preferential oxidation of CO in presence of hydrogen (PROX). The influence of Cu in the cryptomelane structure was evaluated by several characterization techniques such as: X-ray fluorescence (XRF), thermogravimetric analysis (TGA), hydrogen temperature programmed reduction (TPR-H_2) and X-ray photoelectron spectroscopy (XPS). The Cu-modified manganese oxide material (OMS-Cu) showed very high catalytic activity for CO oxidation in comparison to the bare manganese oxide octahedral molecular sieve (OMS). The improved catalytic activity observed in OMS-Cu catalyst was associated to a high lattice oxygen mobility and availability due to the formation of Cu—Mn—O bridges. In addition, under PROX reaction conditions the catalytic activity considerably decreases in the presence of 10% (v/v) CO_2 in the feed while the same amount of water provokes an improvement in the CO conversion and O_2 selectivity.

© 2012 Elsevier B.V. All rights reserved.

1. Introduction

Catalytic carbon monoxide oxidation is an important process in a number of applications including respiratory protection, CO gas sensors, CO_2 lasers, and automotive exhaust treatment [1,2]. In addition, due to the actual interest in proton exchange membrane fuel cell (PEMFC) technology, the preferential oxidation of CO in presence of hydrogen (PROX) has become a relevant technological and environmental application of this catalytic reaction [3,4]. The PROX process constitutes a key step in the H_2 fuel clean-up process for feeds coming from reforming reactions aiming at ensuring a high purity of hydrogen (CO concentration below 10 ppm). Catalysts based on noble metals nanoparticles (e.g. Pt, Ru and Au) supported on reducible metal oxides present high catalytic activity for CO oxidation [1,5]. Nevertheless, the high cost of precious metals has addressed the research on this topic to look for alternative catalysts. Considerable efforts have been directed toward the design of CO oxidation catalysts based on transition metal oxides or composite transition metal oxides.

Cryptomelane-type manganese dioxide materials have been found as effective catalysts for different oxidation reactions [6–10]. Cryptomelane, an octahedral molecular sieve, is an allotropic form of manganese oxide having a well-defined 2×2 tunnel structure (OMS-2) consisting in double chains of edge-shared MnO_6 octahedra and corner-sharing of the double chains (general formula $K_xMn_8O_{16}$). The pore size of the tunnel is 0.46 nm [11]. The average manganese oxidation state in cryptomelane is around 3.8 resulting from the presence of mainly Mn^{4+} and only small amounts of Mn^{3+} and Mn^{2+}. Potassium aqua-complex ions are situated inside the tunnels to provide charge balance and to stabilize the structure. The enhanced catalytic properties of this kind of materials have been associated with their porosity, tunnel structures, degree of crystallinity, reducibility and average oxidation state of the manganese atoms [6,8]. OMS-2 materials doped by metal cations such as Cu [7,12,13], Co [7,12], Ag [12,14,15], Ti [16], Ce [17], Zr [18], V [19] and Pb [20] have been also successfully applied to the oxidation of CO [12,14,15,20]. The improved catalytic properties observed in these materials were correlated with an enhanced lattice oxygen mobility and reactivity due to the interaction of the dopant cation with the manganese oxide structure [7,14,15]. However, the nature of the modification induced by the presence of the dopant cation in the crytomelane structure and the determination of the active sites still remains an unresolved subject.

In our previous work [7], the synthesis and characterization of a series of metal transition-doped OMS-2 structures (Cu^{2+}, Co^{2+}, Ni^{2+} and Zn^{2+}) dedicated as active catalysts in the preferential oxidation of CO in the presence of hydrogen was reported. The material modified with copper was shown to be the most active. This tendency was correlated with the reducibility and the lattice oxygen availability promoted by the presence of the dopant cation in the oxide

* Corresponding author. Present address: Université de Lyon, Institut de Recherches sur la Catalyse et l'Environnement de Lyon, UMR 5256, CNRS, Université Claude Bernard Lyon 1, 2 Avenue A. Einstein, F-69626 Villeurbanne, France.
E-mail address: yesid.hernandez@ircelyon.univ-lyon1.fr (W.Y. Hernández).

0926-3373/$ – see front matter © 2012 Elsevier B.V. All rights reserved.
http://dx.doi.org/10.1016/j.apcatb.2012.04.024

structure. In addition, the remarkable catalytic activity shown by Cu-doped cryptomelane catalyst was also related to the presence of finely dispersed CuO species as a very active phase for CO oxidation [21].

In the present work, we have focused on the physicochemical characterization of the Cu-modified OMS-2 materials synthesized by milling method, and their catalytic activity in the total oxidation of carbon monoxide reaction. In addition, considering the promising results already reported for this material in the PROX reaction [7] and the actual relevance of this catalytic process from environmental and technological point of view, the activity and selectivity of Cu-modified OMS-2 catalysts were here evaluated using more "realistic" PROX reaction conditions. The influence of the presence of 10% (v/v) CO_2 and/or 10% (v/v) H_2O in the reactive stream on the catalytic efficiency was therefore investigated.

2. Experimental

2.1. Synthesis

Cryptomelane oxides were prepared by solid-state reaction between Mn^{7+} and Mn^{2+} species in a high-energy ball milling with stainless steel balls and jar, as described elsewhere [6,7,22]. In a typical experiment, $KMnO_4$ (Panreac 99.0%) and $Mn(CH_3COO)_2{\cdot}4H_2O$ (Panreac 99.0%) (stoichiometric ratio 2:3) were mixed homogeneously and then milled for 1 h at 300 rpm. The resulting black solid was kept 4 h in a capped bottle at 80 °C. The obtained product was thoroughly washed with water until neutrality, dried at 80 °C overnight and finally calcined at 450 °C for 2 h (OMS). Cu-modified cryptomelane (OMS-Cu) was obtained by adding the corresponding metal acetate ($Cu(CH_3COO)_2{\cdot}H_2O$ Sigma–Aldrich > 98.0%) to the $KMnO_4$ and $Mn(CH_3COO)_2{\cdot}4H_2O$ mixture during the milling. The $Cu^{2+}/(Cu^{2+} + Mn^{2+})$ molar ratio employed was 0.1.

2.2. Characterization

The chemical analysis of the samples was performed by X-ray fluorescence spectrometry (XRF) in a Panalytical AXIOS PW4400 sequential spectrophotometer with a rhodium tube as the source of radiation.

Thermogravimetric analysis (TGA) and differential scanning calorimetry (DSC) were employed to study the thermal behavior of the samples. The experiments were performed with a TA Instrument model SDT Q600. The samples were heated from room temperature to 900 °C (10 °C/min^{-1}) in a nitrogen atmosphere (100 mL/min^{-1}). The heat flow data were dynamically normalized using the instantaneous weight of the sample at the respective temperature.

A homemade apparatus was used for obtaining the TPR profiles of the catalysts. In a typical experiment, about 50 mg of solid was loaded in a U-shaped quartz reactor and submitted to a gas mixture flow constituted by 5% hydrogen in Ar at 50 mL/min^{-1}, and then heated from room temperature to 900 °C at 10 °C/min^{-1}. A molecular sieve 13× was used to retain the reduction products, mostly H_2O and CO_2. The effluent gases were analyzed by means of a TCD detector. Hydrogen consumption was determined upon calibration of the system with CuO (Strem Chemicals, 99.999% Cu).

X-ray photoelectron spectroscopy (XPS) analyses were performed on a SSX 100/206 photoelectron spectrometer from Surface Science Instruments (USA) equipped with a monochromatized microfocused Al X-ray source (powered at 20 mA and 10 kV). The samples powders pressed in small stainless steel troughs of 4 mm diameter were placed on a ceramic carousel. The pressure in the analysis chamber was around 5×10^{-9} Torr. The analyzed area was approximately 1.4 mm^2 and the pass energy was set at 150 eV. In these conditions, the resolution determined by the full width at half maximum (FWHM) of the Au $4f_{7/2}$ peak was around 1.6 eV. A flood gun set at 10 eV and a Ni grid placed 3 mm above the sample surface were used for charge stabilization. The following sequence of spectra was recorded: survey spectrum, C 1s, O 1s together with Mn 3s, Mn 2p, Fe 2p, Cu 2p, K 2p and C 1s again to check the stability of charge compensation in function of time and the absence of degradation of the sample during the analyses. The binding energies were calculated with respect to the C—(C,H) component of the C 1s peak fixed at 284.8 eV. Data treatment was performed with the CasaXPS program (Casa Software Ltd, UK). The spectra were decomposed with the least squares fitting routine provided by the software with a Gaussian/Lorentzian (85/15) product function and after subtraction of a non-linear baseline (Shirley type). Molar fractions were calculated using peak areas normalized on the basis of acquisition parameters and sensitivity factors provided by the manufacturer.

2.3. Catalytic activity

For the TOX reaction, the catalysts were pretreated in a 30 mL/min activation flow of 21% O_2 balanced in He. The light-off curves (from room temperature to 450 °C, 5 °C/min) were obtained with a 42 mL/min reactive stream of 3.4% CO (Air Liquide, 99.997%) and 21% O_2 (Air Liquide, 99.999%) in He (Abelló Linde, 99.999%). The reaction was carried out in a conventional continuous flow U-shaped glass reactor working at atmospheric pressure where 80 mg of sample was placed between glass wool. The reaction was followed by mass spectrometry (Balzers® Thermostar).

Preferential oxidation of CO in the presence of hydrogen reactions were carried out at atmospheric pressure in a stainless steel fixed bed reactor (inner diameter of 0.9 cm) with 100 mL/min of a reaction feed, composed by 2% CO (Air Liquide, 99.997%), 1% O_2 (Air Liquide, 99.999%), 50% H_2 (Abelló Linde, 99.999%) and N_2 (Abelló Linde, 99.999%) as balance. The catalyst (100 mg, $100 < \phi < 200$ μm) was diluted in crushed glass of the same particle size, enough to obtain a bed height of 0.5 cm. Prior to all catalytic measurements, the samples were treated in a 21 vol.% O_2/N_2 mixture at 300 °C for 1 h. Products and reactants were separated and quantified by online gas chromatography (Agilent 7890A), employing Haysep Q®, Porapak Q® and molecular sieve columns.

The influence of CO_2 and H_2O on the catalytic activity was investigated by co-introducing 10% CO_2 and/or 10% H_2O in the reaction mixture.

The CO conversion, O_2 conversion and O_2 selectivity were calculated using the following formulas:

$$\text{CO conversion}\,(\%) = \frac{[CO]_{in} - [CO]_{out}}{[CO]_{in}} \times 100. \quad (1)$$

$$O_2\ \text{conversion}\,(\%) = \frac{[O_2]_{in} - [O_2]_{out}}{[O_2]_{in}} \times 100. \quad (2)$$

$$O_2\ \text{selectivity}\,(\%) = \frac{[CO]_{in} - [CO]_{out}}{2([O_2]_{in} - [O_2]_{out})} \times 100. \quad (3)$$

According to the statistics treatment applied to all the data points presented (error of twice the standard error of several analyses), the catalytic curves obtained represent roughly a 95% of confidence interval.

3. Results and discussions

3.1. Chemical analysis

The XRF results obtained for the synthesized solids are presented in Table 1. The presence of iron, coming from the balls and jar used in the milling, was detected in both materials with and without added copper. Nevertheless, it is very interesting to

Table 1
Chemical composition and textural properties of the synthesized materials.

Code	Atomic ratios (XRF)			
	K/M_T	Cu/M_T	Fe/M_T	$Fe+Cu/M_T$
OMS	0.084	–	0.13	0.13
OMS-Cu	0.082	0.042	0.06	0.11

M_T = Fe + Cu + Mn.

observe that the Fe/M_T ratio calculated for the OMS solid decreases with the introduction of Cu during the milling process, while the $Fe + Cu/M_T$ ratio remains almost constant. The cryptomelane structure can host, by this synthetic route, a maximum amount of dopant cations, whatever their nature. This result suggests that the presence of the metal transition cation (used as dopant) in coexistence with the manganese oxide structure (Fe^{3+} and/or Cu^{2+}) could be described by two principal mechanisms: (i), the isomorphic substitution of Mn^{n+} in the parental cryptomelane structure and/or (ii), the replacement of the K^+ ions into the channels of the material. Nevertheless, the presence of CuO and/or Fe_2O_3 segregated phases cannot be discarded.

Considering that OMS and OMS-Cu materials showed a comparable K/M_T ratio (similar structural charge-compensation) and similar crystallographic parameters [7], it is very difficult to assign the exact position occupied by Fe and/or Cu in the cryptomelane structure. In a similar way, for a OMS-2 structure doped with W, Calvert et al. [23] established that the insertion of the dopant cation in the octahedral positions of the network oxide does not provoke major changes in the lattice parameters or atomic coordinates of the doped oxide. This result was explained by the low concentration of W in the materials and the comparable ionic radii of the implied ions occupying octahedral coordination positions. Thus, a similar tendency could be expected for the materials studied in this work, taking into account the low incorporation of the dopant cations and the similar crystals radii of Fe and Cu ions in eight-fold coordination [24]. Additional experiments are required to further investigate this working hypothesis.

3.2. Thermal stability

The thermal stability of the synthesized solids was evaluated by thermogravimetric analysis and differential scanning calorimetry. Fig. 1a displays the TGA results obtained for OMS and OMS-Cu materials. In the analyzed temperature range (30–900 °C) it is possible to observe at least four weight loss zones, very similar in both solids. The first weight loss, about 5% at ≤250 °C, can be attributed to the depletion of physisorbed and chemisorbed water [22]. The second one, ~3% occurring between 300 and 550 °C, can be ascribed to two different processes: (i) the loss of water inside the (2×2) tunnels and (ii) the desorption of structural oxygen close to the surface, related with the formation of lattice vacancies without decomposition of the material [25].

Finally, the third and fourth weight loss observed in the studied solids (550–640 °C and >600 °C, respectively) implies oxygen depletion from the structure of the material and their subsequent decomposition to bixbyite (Mn_2O_3) and then, to hausmannite (Mn_3O_4) [26,27].

The maximum temperature values associated with the weight loss processes were estimated from the respective DTG curves (Fig. 1b) and results are presented in Table 2. Except for the thermal event at 95 °C, associated with the loss of water (peak I), all the thermal processes related with the depletion of oxygen appears about 20 °C lower for OMS-Cu solid in comparison to OMS one. These thermal processes are well correlated with the endothermic peaks at the same temperature, observed in the DSC curves (Fig. 1b). Hence, considering that the textural properties and crystal structures of the

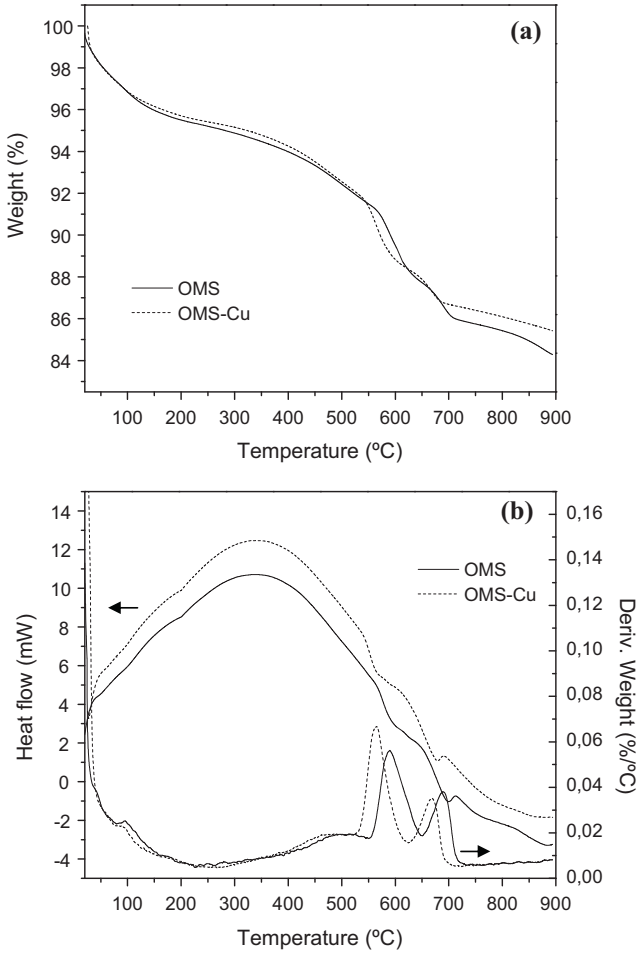

Fig. 1. Thermal profiles obtained for the studied materials. (a) Thermogravimetric analysis (TGA) and (b) differential thermal analysis (DTA)/differential scanning calorimetry (DSC).

studied materials are basically the same, the presence of Cu^{2+} in the cryptomelane structure promotes the mobility and availability of the lattice oxygen in comparison to OMS oxide.

3.3. Temperature programmed reduction (TPR-H_2)

The TPR-H_2 profiles obtained for the studied materials are presented in Fig. 2. The reduction processes characteristic of the cryptomelane structure have been described elsewhere [7,28,29]. The lowest temperature reduction process corresponds to the consumption of structural oxygen close on the surface, without decomposition of the material (generation of oxygen vacancies). Then, successive manganese oxide reductions occur as follows: $MnO_2 \rightarrow Mn_2O_3 \rightarrow Mn_3O_4 \rightarrow MnO$ [28]. Nevertheless, the number and intensity of the peaks on the TPR profiles can also depend on the different local environments of such species and the presence of other reducible ones. Below 500 °C, OMS material showed the four peaks characteristic of the reduction processes described above, at 191, 259, 301 and 354 °C. In addition, a broad and low intense

Table 2
Assignation peaks from TGA measurements.

Code	Temperature peak (°C)			
	Peak I	Peak II	Peak III	Peak IV
OMS	95	498	589	690
OMS-Cu	95	472	565	667

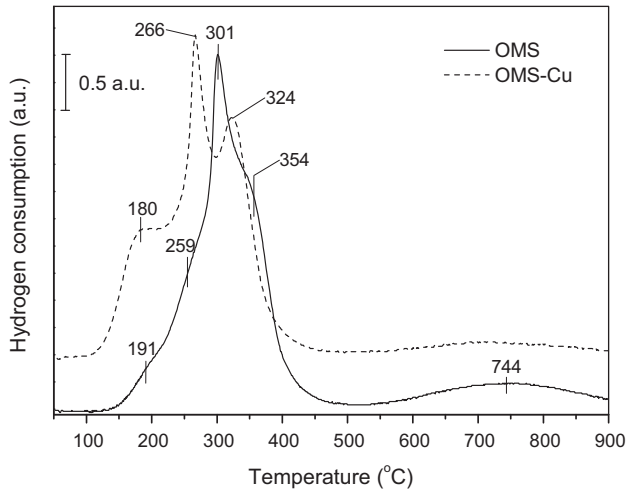

Fig. 2. Temperature programmed reduction profiles (TPR) for the synthesized materials.

hydrogen consumption peak can be observed between 550 and 900 °C, with a maximum centered at about 744 °C (Fig. 2). This high temperature reduction process can be related to the presence of Fe in the structure (incorporated as an impurity during the synthesis), considering that the reduction of Fe_3O_4 to FeO, and later to metallic Fe, have been described in a similar interval of temperature [30,31]. On the other hand, all the reduction processes observed in the OMS-Cu solid were shifted to lower temperature values in comparison to OMS oxide. These data suggest that the amount of structural oxygen available to react with the hydrogen in the gas phase is strongly influenced by the presence of Cu^{2+} in the synthesized material, which is in a good agreement with the results observed by thermogravimetric analysis (Section 3.2). This fact may be connected to the formation of Mn—O—Cu bridges where a high oxygen lability is promoted by the electronic delocalization induced by the presence of Cu [7]. Similar results have been found for Ag^{+}-OMS-2 [12,14,15], Cu^{2+} and Co^{2+}-OMS-2 [12] and MnO_2–CuO mixed oxide materials [32] and correlated with their catalytic activities. In addition, the presence of Cu in OMS-Cu catalyst can produce spillover hydrogen species [33], which are able to accelerate the reduction of the Mn^{x+} cations characteristic of the cryptomelane structure.

On the other hand, the reduction process observed at 744 °C on OMS oxide is almost absent in the TPR profile of the OMS-Cu sample, which agrees with the low Fe incorporation on the Cu-doped material, as discussed in Section 3.1.

The average oxidation state (AOS) was calculated for Mn in the studied materials (according to its hydrogen consumptions), and assuming Mn^{2+} as the final oxidation state [34]. The obtained AOS values for OMS and OMS-Cu materials (3.7 and 3.6, respectively) appeared to be very close to that commonly reported in the literature for this kind of materials (~3.8) [6,26,35]. Therefore, the presence of Cu and/or Fe in the cryptomelane structure does not have a significant effect on the Mn^{4+}/Mn^{3+} ratio of the synthesized materials.

3.4. XPS analysis

3.4.1. O 1s spectra

Fig. 3 shows the O 1s spectra of the studied materials. According to the peak positions, three types of oxygen species can be identified: the low binding energy peak, O_I, which is ascribed to lattice oxygen (O^{2-}), the medium binding energy peak, O_{II}, assigned to surface adsorbed oxygen (O_2^- or O^-), ^-OH groups and oxygen vacancies; and finally the high binding energy peak, O_{III}, likely

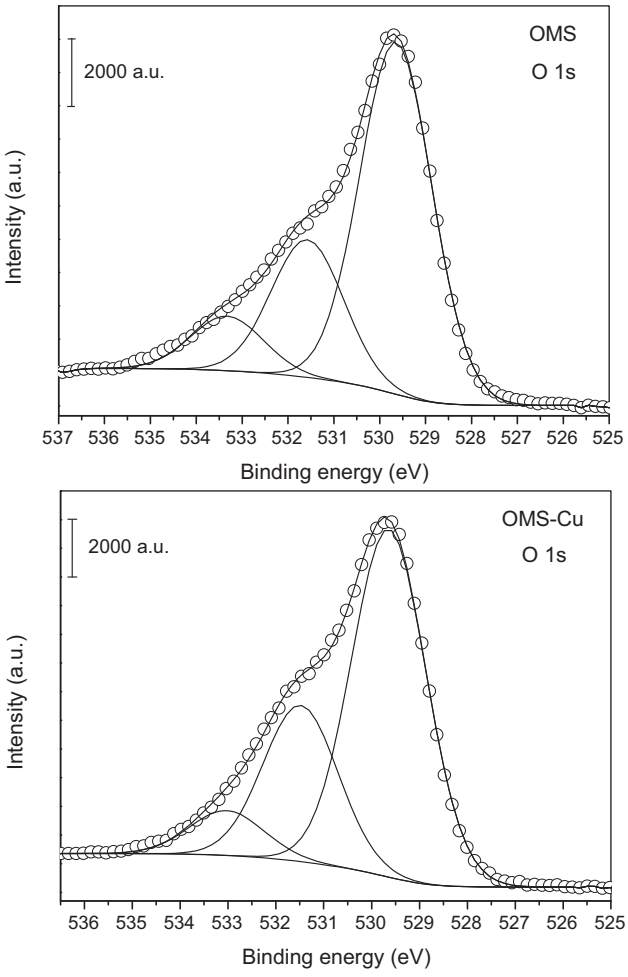

Fig. 3. O 1s XPS spectra of OMS and OMS-Cu solids.

associated with adsorbed molecular water [20,36,37]. The peak positions and relative abundance of O_I, O_{II} and O_{III} species are listed in Table 3. The principal component corresponds to the lattice oxygen, followed by the peak O_{II} of adsorbed oxygen and O_{III} of adsorbed water. As can be observed, the amount of lattice oxygen is very close in both materials because their crystalline structures are identical. Nevertheless, considering that the BET surface area of OMS and OMS-Cu solids is practically the same (124 and 117 m^2/g, respectively), the relative abundance of the O_{II} and O_{III} species calculated for them is different. In this way, the amount of O_{II} species on the OMS-Cu solid is higher in comparison to the OMS solid, while the surface concentration of water (O_{III} species) is lower. As was described before, the nature of the O_{II} species in these materials can be related to the presence of oxygen vacancies. The interaction of these point defects with molecular oxygen and/or water provokes the generation of peroxides, superoxides and hydroxyl species [38–41]. Thus, a higher surface oxygen vacancies concentration in OMS-Cu solid can be expected, considering that the insertion of Cu in the oxide structure enhances the oxygen lability and reducibility of the material. This explains why an increment in

Table 3
Oxygen species proportion and binding energy obtained from XPS analysis (O 1s).

Code	O_I		O_{II}		O_{III}	
	Pos. (eV)	%Area	Pos. (eV)	%Area	Pos. (eV)	% Area
OMS	529.6	64.6	531.6	25.3	533.3	10.0
OMS-Cu	529.6	63.3	531.5	28.5	533.0	8.1

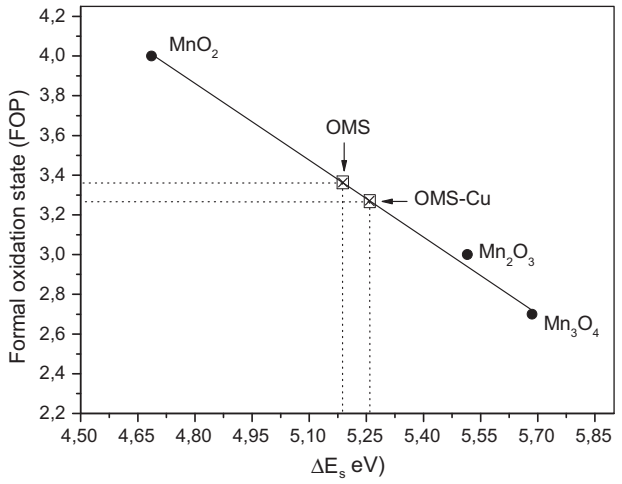

Fig. 4. Relationship manganese formal oxidation state (FOS) and Mn 3s XPS splitting.

the O_{II} species concentration was observed. This result is in a good agreement with the lower amount of molecular adsorbed water (from the environment) on the OMS-Cu solid, where an enhanced oxygen vacancies concentration facilitates the dissociation of the adsorbates [41,42]. In this way, the concentration of $^{-}$OH species was increased concurrently with the dissociation of the molecular adsorbed water on the oxygen vacancies.

3.4.2. Mn 3s spectra

The formal oxidation state (FOS) of manganese was determined by XPS analysis based on a correlation between the relative energy between the main peak and the satellite peak of the Mn 3s signal (ΔE_s) and the FOS reported elsewhere [9,43–45]. Fig. 4 shows the variation of the formal oxidation state of manganese with the relative energy between the main peak and the satellite peak of the Mn 3s signal in the studied catalysts and some reference manganese oxides. The FOS values obtained for OMS and OMS-Cu materials were 3.4 and 3.3, respectively. These values tend to be lower in comparison to the average oxidation state commonly reported in the literature for manganese oxides with cryptomelane-type structure (from 3.7 to 3.9) [6,26,35,46]. However, the AOS values calculated for OMS and OMS-Cu solids by the hydrogen consumption coming from the H_2-TPR analysis showed to be closer to the expected ones (3.7 and 3.6, respectively). This means that Mn atoms in the oxide structures are mostly in the Mn^{4+} state, with minor amounts in the Mn^{3+} state, and/or Fe^{3+}/Cu^{2+} species replacing Mn positions into the cryptomelane structure. Taking into account the structural features discussed before for these materials, the unexpected low FOS values obtained by XPS technique could be explained considering two facts: (i) a tendency of the materials to be reduced under ultra high vacuum conditions, considering the high oxygen lability induced by the presence the dopant cations (especially for the OMS-Cu solid) and (ii) a particular Mn 3s exchange splitting due to the insertion of Fe and/or Cu into the cryptomelane structure. For mixed-valence manganite materials, Galakhov et al. [43] have reported that the increase of the degree of Mn—O covalence as well as the increase of the formal valence of Mn ions should lead to smaller Mn 3s splitting. Otherwise, for the materials studied in this work, the presence of Fe and/or Cu in the material's structure can provoke the weakening of the Mn—O bond by electronic delocalization on the Mn—O—Cu bridges [7,47]. Consequently, the charge-transfer satellites for the Mn 3s spectra become less important and the separation between the peaks is changed (Mn 3s splitting increases). For this reason, the FOS value obtained from the analysis of Mn 3s spectra appears to be lower in comparison to the AOS value calculated by H_2-TPR analysis and also proves the beneficial effect of the dopant cations on the oxygen mobility and redox properties of the cryptomelane structure

Table 4
Binding energies obtained from XPS analysis of Fe 2p and Cu 2p levels.

Code	Fe 2p (eV)		Cu 2p (eV)	
	1/2	3/2	1/2	3/2
OMS	724.5	710.9	–	–
OMS-Cu	724.4	710.9	952.6	932.8

3.4.3. Cu 2p and Fe 2p spectra

The oxidation states of Cu and Fe, associated to the cryptomelane structure in OMS and OMS-Cu materials, were also analyzed by XPS technique. Table 4 summarizes the peak position of the studied elements. From the binding energies and characteristic doublet separation obtained for the 2p level in Cu and Fe, the mainly cationic species present in the cryptomelane structure correspond to Cu^{2+} and Fe^{3+} [48]. One could suggest that the presence of these elements in their highest oxidation states can facilitate their replacement by Mn^{4+} in the cryptomelane structure (close ionic radius). However, as was discussed in Section 3.1, is very difficult to assign the exact position occupied by Fe and/or Cu in the material structure only with the characterization discussed in this work.

3.5. Catalytic activity

3.5.1. Total oxidation of CO (TOX)

The catalytic activity of the studied materials for the total CO oxidation as a function of reaction temperature is shown in Fig. 5. As can be observed, the presence of copper in the oxide structure has a very strong influence on the catalytic activity of OMS-Cu solid even at room temperature. Therefore, while the OMS catalyst reaches ~30% CO conversion at 25 °C, the OMS-Cu solid achieves the total combustion of carbon monoxide at the same temperature. In general, the modification of OMS-type structures by the presence of different dopant cations has been postulated as a good alternative to improve their catalytic activity for catalytic oxidation reactions [7,13–15,17,49]. In those works, the enhanced reactivity of the catalysts was associated with the reducibility and oxygen reactivity induced by the presence of the dopant cations in the oxide structure [28,47,50]. In particular for Cu doped OMS materials, a very strong improvement of the catalytic activity and stability properties have been discussed in the literature [7,12,13,47,51] and related to the redox properties of highly dispersed CuO and Cu_2O oxides

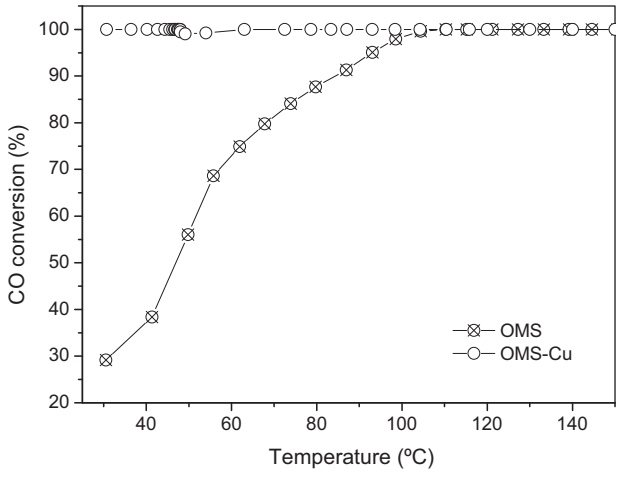

Fig. 5. Total oxidation of CO (TOX) over OMS and OMS-Cu oxides.

and the electronic delocalization on the Mn—O bond induced by the Cu^{2+} ions. In a recent report, Liu et al. [13] proposed that the CO oxidation on a CuO/OMS-2 catalyst may follows the Mars-van-Krevelen mechanism with a Cu^{2+}–O^{2-}–Mn^{4+} ↔ Cu^{+}–□–Mn^{3+} + O_2 redox couple involved (□ representing an oxygen vacancy). The highly reducible bridge oxygen in the Cu^{2+}–O^{2-}–Mn^{4+} entity could react with CO to produce CO_2 and a partially reduced Cu^{+}–□–Mn^{3+} couple; then the Cu^{+}–□–Mn^{3+} entities could be re-oxidized rapidly by O_2 in the feed gas. A similar mechanism was proposed by Xia et al. [12] for OMS-2-type structures doped with M = Cu^{2+}, Co^{2+} or Ag^{+}, but considering the reduction and reoxidation of the dopant cation into the tunnels, together with the Mn^{4+} from the oxide structure in a complete redox cycle. Therefore, according to the structural characterization described for the OMS-Cu solid, the CO molecule can react with the labile oxygen species induced by the presence of Cu in the structure, and the resulting oxygen vacancies can be removed by adsorption of the oxygen molecules coming from the gas phase [7].

On the other hand, because in OMS material an important Fe incorporation occurs during the preparation of the sample, is also necessary to keep in mind its influence in the catalytic activity of such material. In that way, as was described before for the OMS-Cu material, the formation of a reducible bridge type Fe^{3+}–O^{2-}–Mn^{4+} is also possible in OMS catalyst. Nevertheless, its influence in the total oxidation of CO at temperatures below 100 °C is not as relevant as was obtained with OMS-Cu catalyst (Fig. 5). This result could be related with two main facts associated to the chemical nature of the foreign cations: firstly, the higher electronegativity of Cu in comparison to Fe (1.9 and 1.8, respectively), which causes a higher electron delocalization on the bridge M—O—Mn. This effect improves the oxygen availability coming from lattice oxide, and as consequence, its reactivity [7]. Second, an enhanced CO adsorption on the Cu sites of the catalyst should be also considered in the case of OMS-Cu catalyst against OMS one [52].

3.5.2. *Preferential oxidation of CO in presence of hydrogen (CO-PROX)*

A lot of papers have been published on the PROX reaction. Moreover most of them report studies without CO_2 and steam in the reactant feed, which makes limited the information obtained from them. Considering the relatively high concentration of CO_2 and H_2O present in a real reformate off-gas, the catalyst performance and durability can be affected. The presence of these compounds may produce several effects, such as: coverage of active sites, thus, decreasing catalyst activity, and/or the simultaneous occurrence of other reactions such as forward and reverse WGS, or methanation [53].

In order to explore these possibilities, the catalytic performance of OMS-Cu catalysts was evaluated under four different reaction conditions: (i) in the absence of CO_2 and H_2O (ideal conditions), (ii) in the presence of 10% CO_2, (iii) in the presence of 10% H_2O, and (iv) in the presence of both 10% CO_2 and 10% H_2O in the feed.

3.5.2.1. Feed free of CO_2 and H_2O. Fig. 6 depicts the CO conversion and O_2 selectivity obtained for the studied materials under ideal PROX reaction conditions. In general, the CO conversion observed for OMS and OMS-Cu materials is significantly decreased compared with the catalytic activity observed under TOX reaction conditions (Fig. 5). This difference is as expected considering the difference in the CO/O_2 ratios employed in each process, the space velocity and, of course, the complexity of the PROX process due to the presence of a high hydrogen concentration. Nevertheless, as it was observed in TOX reaction, the OMS-Cu catalyst showed an enhanced catalytic activity in PROX reaction conditions in comparison to OMS one. At temperatures higher than 140 °C on the material modified with Cu, the CO conversion reaches values higher than 70% while the O_2 selectivity gradually decreases for increasing temperature (Fig. 6). The results obtained for the OMS-Cu catalyst in PROX reaction in the absence of CO_2 and H_2O have been already described and compared with other transition metal doped OMS-2 structures and the undoped material [7]. The modification of the cryptomelane structure by the presence of Co^{2+} and especially Cu^{2+} has a significant effect on the catalytic activity of these materials. Considering the improved reducibility and redox activity shown by the Cu-modified OMS-2 material, this catalyst has been selected to evaluate the influence of the feed composition in the catalytic properties of the OMS systems.

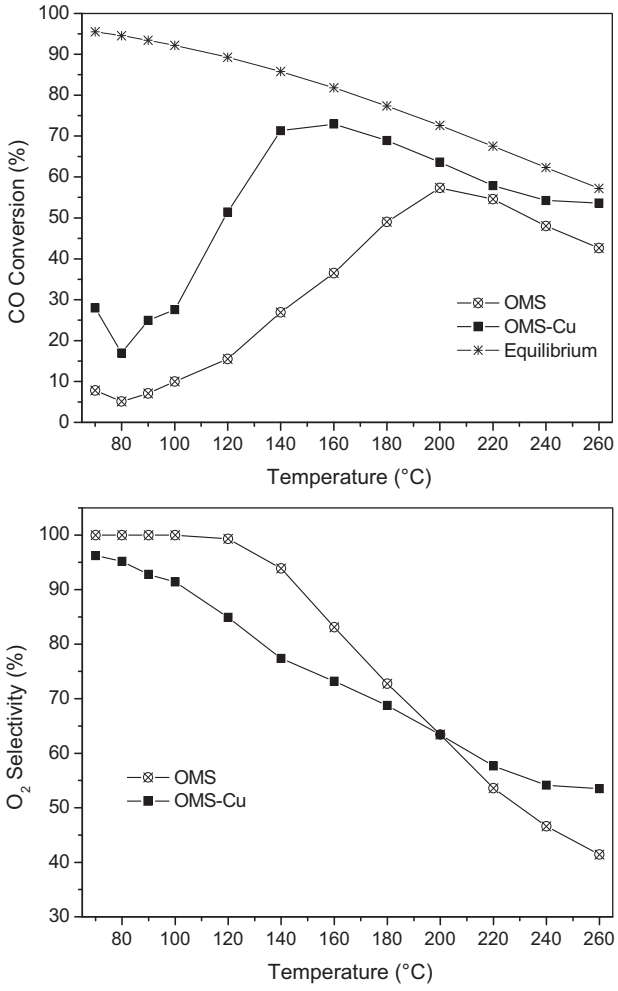

Fig. 6. Variation of CO conversion and O_2 selectivity as a function of the temperature reaction for the preferential oxidation of CO in presence of hydrogen (PROX), over OMS and OMS-Cu materials.

3.5.2.2. Effect of CO_2 addition. The effect of adding 10 vol.% CO_2 in the dry feed stream was evaluated. The CO and O_2 conversions were significantly decreased at temperatures lower than ~200 °C (Figs. 7 and 8). For higher temperatures the CO conversion was equal to that obtained in ideal conditions due to the limitation imposed by the equilibrium condition [7]. In both cases the maximum CO conversion was reached when the O_2 conversion was close to 100%. However, in presence of CO_2, the maximum CO conversion decreases ~10%, while its associated temperature increases of ~20 °C in comparison to the reaction in ideal conditions. On the other hand, the O_2 selectivity does not seem to be affected by the presence of CO_2 (Fig. 9). However, because the observed CO conversion was quite different in these conditions, the competition between CO and H_2 for the O_2 molecules occurs at different reactive

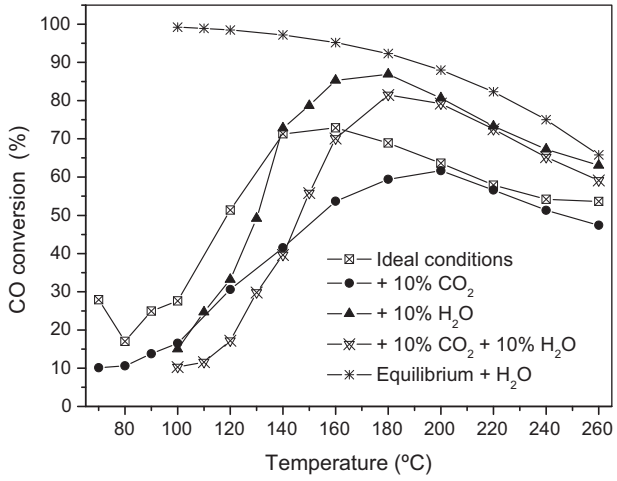

Fig. 7. Effect of the feed composition on the CO conversion of OMS-Cu catalyst, under PROX reaction conditions. Ideal conditions: 2% CO, 1% O_2, 50% H_2 and He as balance.

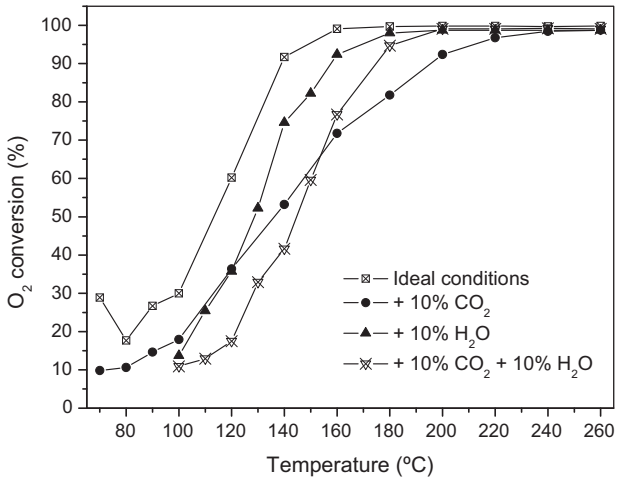

Fig. 8. Effect of the feed composition on the O_2 conversion of OMS-Cu catalyst, under PROX reaction conditions.

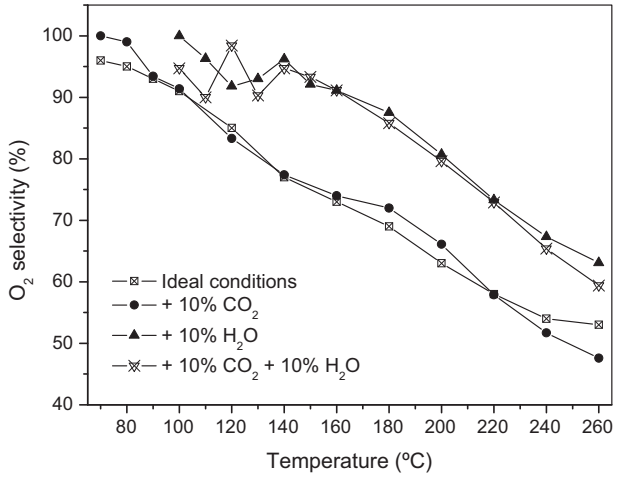

Fig. 9. Effect of the feed composition on the O_2 selectivity of OMS-Cu catalyst, under PROX reaction conditions.

partial pressures and a direct comparison cannot be done. At higher temperatures, the hydrogen combustion is mostly favored by the thermodynamics.

In general, the presence of CO_2 in the feed during the PROX reaction has been found to be detrimental due to the blocking effect of the CO_2 on the CO adsorption sites and/or formation of carbonate species [54–56]. In the case of the OMS-Cu material tested in this work, the main CO_2 effect seems to be a partial blockage of the active sites where the CO and H_2 adsorption takes place. The origin of the CO_2 blocking effect can be related to the presence of carbonate species already reported over reducible metal oxides [57]. On the other hand, the presence of CO_2 could also affect the O_2 activation on the surface oxygen vacancies, taking into account that the CO_2 interaction with these types of defects has been also reported [58–60]. Although the CO_2 interaction with an oxygen vacancy is usually weaker than that expected for O_2, an increase in the partial pressure of CO_2 can prevent the oxygen activation on a defective surface material [61] and then, decreases its catalytic activity.

3.5.2.3. Effect of H_2O. As can be seen in the Fig. 7, depending on the reaction temperature, the presence of 10% H_2O has a detrimental or beneficial effect on the CO conversion in comparison to dry conditions. In that sense, for temperatures between 100 and 120 °C, the steam provokes the decrease of the CO conversion in a similar proportion as was observed in the presence of CO_2. For temperatures higher than 140 °C, the CO conversion increases and reaches values higher than those observed when the feed was free of water, together with a shift in the temperature of the maximum CO conversion (~85% conversion at 160 °C). At higher temperatures, the CO conversion is close to the value expected from the thermodynamic equilibrium (considering the presence of water in the feed).

In addition, the O_2 selectivity under these reaction conditions (Fig. 8) was considerably enhanced for all reaction temperatures in comparison to the process under ideal conditions and in presence of CO_2.

Different effects have been reported in the literature for the PROX reaction in the presence of steam. On $Au/MnO_x/Al_2O_3$ catalyst, Grisel and Nieuwenhuys [62] observed the inhibition of the catalytic activity, and suggested that H_2O poisons the oxygen vacancies presented in the MnO_x support. For CuO/CeO_2 catalysts, Won Park et al. [55] propose that H_2O can be adsorbed on the CO adsorption sites inhibiting the catalyst activity.

On the other hand, for Pt/Al_2O_3 catalysts, the activity has shown to be unaltered or slightly enhanced by the presence of steam [63–65], or even notoriously enhanced [57]. In the last case, the authors suggest three possible explanations for this effect: (i) water enhances the water gas shift reaction and as a result, more CO is converted to CO_2, (ii) hydroxyl groups formed on the catalyst upon adsorption of water are a better oxidant than oxygen and increase the oxidation rate of CO and hydrogen and (iii) the modification of the $Pt^0/Pt(O)_x$ ratio by the presence of water modifies the catalytic activity of the systems. In addition, for OMS-2 materials doped with Co, Cu and Ag, Xia et al. [12] showed that the presence of water in the feed does not affect the stability of the catalyst during long time reaction (up to 30 h) under carbon monoxide oxidation conditions.

Besides that, the effect of the water on the thermal stability of the carbonate species formed on the catalyst surface should be also considered. In this way, several works on gold-based catalysts have reported that the presence of steam in the reaction mix improves the decomposition rate of the carbonate species due to the formation of bicarbonate species, which are characterized by a low thermal stability [66,67]. Thus, the actives sites on the catalyst surface are quickly regenerated and the rate of the CO oxidation reaction results to be improved.

For the OMS-Cu catalyst studied in this work, the steam effect on the PROX reaction can be explained considering different facts. First, at low reaction temperatures, the H_2O can block the active sites on the catalyst surface, such as it occurs in the presence of CO_2. However, with the increase of the temperature, two special situations could be considered: (i) the improvement of the water gas shift reaction kinetics would result in an over-consumption of carbon monoxide together with the production of hydrogen and carbon dioxide. As a consequence, an increase in the O_2 selectivity should be expected. Obviously, the equilibrium of the water gas shift reaction must be affected by the increase of the temperature and the presence of CO_2. (ii) The water dissociation on the surface punctual defects promotes the formation of hydroxyl groups. These groups are able to modify the oxidation rate of CO because they facilitate the formation of intermediary species (bidentate carbonates) during the CO to CO_2 oxidation. Thus, as was discussed above by XPS analysis, the improved water dissociation on the OMS-Cu surface can be considered as responsible of the enhancement in the catalytic properties of the material in presence of 10% H_2O. This positive effect became relevant at higher temperatures, where thermal effects enhance the oxygen vacancies generation.

In addition, Fig. 9 depicts an increment in the O_2 selectivity in all the interval of evaluated temperatures due to the presence of water in the feed, while the O_2 conversion remains lower than that observed under ideal conditions. Thus, one could also consider the effect of the water on the equilibrium of the reverse water gas shift reaction (Eq. (4)), which limits the PROX process from a thermodynamic point of view.

$$H_{2(g)} + CO_{2(g)} \leftrightarrow CO_{(g)} + H_2O_{(g)}. \quad (4)$$

In this way, the presence of water affects the equilibrium of the reaction (4) decreasing the conversion rate of H_2 and CO_2 and, on the other hand, improving the conversion of CO and H_2O. This effect would result in an increment of the CO conversion and a decrease in the H_2 combustion which means an improved O_2 selectivity.

3.5.2.4. Effect of CO_2 and H_2O. In order to check the global effect of the simultaneous water and carbon dioxide presence, an additional experiment was carried out co-adding 10% of CO_2 and 10% of H_2O in the feed. The effect on the catalyst activity depends of the reaction temperature. At temperatures below 140 °C, the CO conversion was inhibited (Fig. 7), obtaining values lower than those observed for CO_2 and H_2O independently added. However, from this temperature the CO conversion was better than that obtained when CO_2 was present in the feed, but worse than those with only water or under ideal conditions. The maximum of CO conversion was lower compared to only water in the feed, but reached the conversion of the thermodynamic equilibrium at the same temperature. So, the clear positive effect of the water is more dominant than the negative effect of CO_2 at reaction temperatures higher than 140 °C. On the other hand, the O_2 selectivity follows a similar trend to that observed by the presence of only H_2O (Fig. 7), suggesting that the rate of H_2 oxidation was affected by the simultaneous presence of CO_2 and H_2O in the same way that when only water exists.

Finally, and in order to evaluate the catalytic performance of the OMS-Cu catalyst under the different reaction conditions tested, the relationship between the CO conversion and O_2 selectivity was depicted in Fig. 10. As was described elsewhere [7], the similar and high O_2 selectivity (higher than 90%) observed at CO conversions below 20% in all the reaction conditions, can be associated with the thermodynamic as the leading factor for the CO and H_2 oxidation, as expected from the enthalpy values of both reactions. However, with the increase of the CO conversion, the behavior started to be quite different depending of the feed composition, and finally it drops at the level imposed by the equilibrium situation (straight line in Fig. 10). In this way, taking as reference

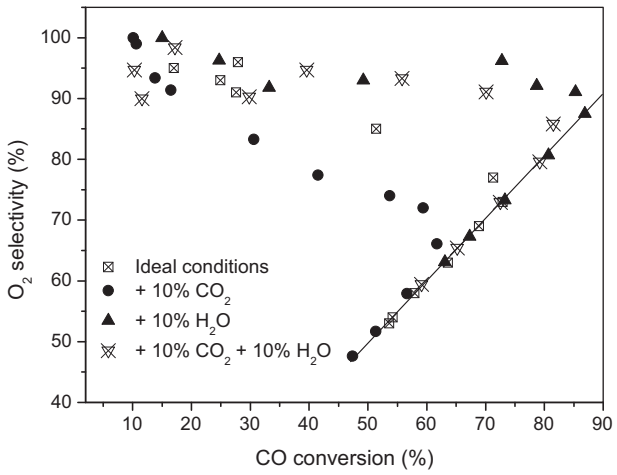

Fig. 10. O_2 selectivity vs. CO conversion as criterion to evaluate the catalytic efficiency of OMS-Cu solid.

the behavior observed for the reaction under ideal conditions, the presence of CO_2 in the stream strongly decreases the O_2 selectivity at the same CO conversion. On the other hand, the presence of water in the feed remarkably enhances the maximum CO conversion keeping stable and high O_2 selectivity, even in presence of CO_2. Thus, for the OMS-Cu catalyst employed in this reaction, the presence of 10% (v/v) of water in the gas phase has a beneficial effect on the catalytic performance of the process and even more, counteracts the detrimental influence observed for the same amount of CO_2. This result looks very interesting from a technological point of view because the efficiency of the catalyst appears to be unaffected or even improved under the real reaction conditions. Nevertheless, additional experiments are necessary in order to establish the stability of this kind of catalysts and the influence of a fluctuating feed composition.

4. Conclusions

OMS-Cu catalyst exhibits very high CO oxidation activity under TOX reaction conditions and relevant CO conversion and O_2 selectivity under PROX ones. The improved catalytic performance of this material can be related with its remarkable oxygen mobility and lability in comparison to OMS catalyst. This feature derives from the interaction Cu–Mn in the lattice oxide due to charge delocalization effects and generation of active sites for CO oxidation reaction. The beneficial effect of water, even in presence of an excess of CO_2 in the feed, is an advantage for the use of this kind of materials in the purification of hydrogen under realistic reformer conditions.

Acknowledgments

Financial support for this work has been obtained from the Spanish Ministerio de Ciencia e Innovación (ENE2009-14522-C05-01) cofinanced by FEDER funds from the European Union and from Junta de Andalucía (P09-TEP-5454). S. Ivanova acknowledges MEC for her contract Ramon y Cajal and W.Y. Hernández thanks the AlBan program of the European Union for the fellowship awarded (E06D101739CO) and Junta de Andalucía for the financial support of his research stay at the Université catholique de Louvain.

References

[1] S. Royer, D. Duprez, ChemCatChem 3 (2011) 24–65.
[2] E.C. Njagi, C.-H. Chen, H. Genuino, H. Galindo, H. Huang, S.L. Suib, Applied Catalysis B 99 (2010) 103–110.
[3] E.D. Park, D. Lee, H.C. Lee, Catalysis Today 139 (2009) 280–290.

[4] N. Bion, F. Epron, M. Moreno, F. Mariño, D. Duprez, Topics in Catalysis 51 (2008) 76–88.
[5] O.H. Laguna, M.A. Centeno, G. Arzamendi, L.M. Gandia, F. Romero-Sarria, J.A. Odriozola, Catalysis Today 157 (2010) 155–159.
[6] M.I. Domínguez, P. Navarro, F. Romero-Sarria, D. Frías, S.A. Cruz, J.J. Delgado, M.A. Centeno, M. Montes, J.A. Odriozola, Journal of Nanoscience and Nanotechnology 9 (2009) 3837–3842.
[7] W.Y. Hernandez, M.A. Centeno, F. Romero-Sarria, S. Ivanova, M. Montes, J.A. Odriozola, Catalysis Today 157 (2010) 160–165.
[8] J.S. Valente, D. Frías, P. Navarro, M. Montes, J.J. Delgado, E. Fregoso-Israel, E. Torres-García, Applied Surface Science 254 (2008) 3006–3013.
[9] I. Barrio, I. Legórburu, M. Montes, M.I. Domínguez, M.A. Centeno, J.A. Odriozola, Catalysis Letters 101 (2005) 151–157.
[10] Y.G. Yin, W.Q. Xu, R. DeGuzman, S.L. Suib, C.L. O'Young, Inorganic Chemistry 33 (1994) 4384–4389.
[11] R.N. DeGuzman, Y.F. Shen, E.J. Neth, S.L. Suib, C.L. O'Young, S. Levine, J.M. Newsam, Chemistry of Materials 6 (1994) 815–821.
[12] G.G. Xia, Y.G. Yin, W.S. Willis, J.Y. Wang, S.L. Suib, Journal of Catalysis 185 (1999) 91–105.
[13] X.-S. Liu, Z.-N. Jin, J.-Q. Lu, X.-X. Wang, M.-F. Luo, Chemical Engineering Journal 162 (2010) 151–157.
[14] W. Gac, G. Giecko, S. Pasieczna-Patkowska, T. Borowiecki, L. Kepinski, Catalysis Today 137 (2008) 397–402.
[15] W. Gac, Applied Catalysis B 75 (2007) 107–117.
[16] H. Nur, F. Hayati, H. Hamdan, Catalysis Communications 8 (2007) 2007–2011.
[17] M. Abecassis-Wolfovich, R. Jothiramalingam, M.V. Landau, M. Herskowitz, B. Viswanathan, T.K. Varadarajan, Applied Catalysis B 59 (2005) 91–98.
[18] R. Jothiramalingam, B. Viswanathan, T.K. Varadarajan, Journal of Molecular Catalysis A 252 (2006) 49–55.
[19] L. Sun, Q. Cao, B. Hu, J. Li, J. Hao, G. Jing, X. Tang, Applied Catalysis A 393 (2011) 323–330.
[20] X. Yang, J. Han, Z. Du, H. Yuan, F. Jin, Y. Wu, Catalysis Communications 11 (2010) 643–646.
[21] C.-S. Chen, J.-H. You, J.-H. Lin, Y.-Y. Chen, Catalysis Communications 9 (2008) 2381–2385.
[22] Y.S. Ding, X.F. Shen, S. Sithambaram, S. Gomez, R. Kumar, V.M.B. Crisostomo, S.L. Suib, M. Aindow, Chemistry of Materials 17 (2005) 5382–5389.
[23] C. Calvert, R. Joesten, K. Ngala, J. Villegas, A. Morey, X. Shen, S.L. Suib, Chemistry of Materials 20 (2008) 6382–6388.
[24] R.D. Shannon, Acta Crystallogaphica A32 (1976).
[25] Y.F. Shen, S.L. Suib, C.L. O'Young, Journal of the American Chemical Society 116 (1994) 11020–11029.
[26] K.A. Malinger, Y.S. Ding, S. Sithambaram, L. Espinal, S. Gomez, S.L. Suib, Journal of Catalysis 239 (2006) 290–298.
[27] J. Luo, Q. Zhang, J. Garcia-Martinez, S.L. Suib, Journal of the American Chemical Society 130 (2008) 3198–3207.
[28] M. Tsuji, S. Komarneni, Journal of Materials Research 8 (1993) 611–616.
[29] L. Christel, A. Pierre, D.A.-M.R. Abel, Thermochimica Acta 306 (1997) 51–59.
[30] G. Neri, A.M. Visco, S. Galvagno, A. Donato, M. Panzalorto, Thermochimica Acta 329 (1999) 39–46.
[31] H.-Y. Lin, Y.-W. Chen, C. Li, Thermochimica Acta 400 (2003) 61–67.
[32] S.B. Kanungo, Journal of Catalysis 58 (1979) 419–435.
[33] J. Ashok, P.S. Reddy, G. Raju, M. Subrahmanyam, A. Venugopal, Energy and Fuels 23 (2009) 5–13.
[34] F. Kapteijn, L. Singoredjo, A. Andreini, J.A. Moulijn, Applied Catalysis B 3 (1994) 173–189.
[35] M.E. Becerra, N.P. Arias, O.H. Giraldo, F.E. López Suárez, M.J. Illán Gómez, A. Bueno López, Applied Catalysis B 102 (2011) 260–266.
[36] V.P. Santos, M.F.R. Pereira, J.J.M. Órfão, J.L. Figueiredo, Applied Catalysis B 99 (2010) 353–363.
[37] K. Jirátová, J. Mikulová, J. Klempa, T. Grygar, Z. Bastl, F. Kovanda, Applied Catalysis A 361 (2009) 106–116.
[38] M.I. Domínguez, F. Romero-Sarria, M.A. Centeno, J.A. Odriozola, Applied Catalysis B 87 (2009) 245–251.
[39] H.T. Chen, J.G. Chang, H.L. Chen, S.P. Ju, Journal of Computational Chemistry 30 (2009) 2433–2442.
[40] F. Romero-Sarria, A. Penkova, L.M. Martinez, T.M.A. Centeno, K. Hadjiivanov, J.A. Odriozola, Applied Catalysis B 84 (2008) 119–124.
[41] R. Schaub, P. Thostrup, N. Lopez, E. Lagsgaard, I. Stensgaard, J.K. Nurskov, F. Besenbacher, Physical Review Letters 87 (2001) 2661041–2661044.
[42] M. Fronzi, S. Piccinin, B. Delley, E. Traversa, C. Stampfl, Physical Chemistry Chemical Physics 11 (2009) 9188–9199.
[43] V.R. Galakhov, M. Demeter, S. Bartkowski, M. Neumann, N.A. Ovechkina, E.Z. Kurmaev, N.I. Lobachevskaya, Y.M. Mukovskii, J. Mitchell, D.L. Ederer, Physical Review B 65 (2002) 1131021–1131024.
[44] C. Cellier, V. Ruaux, C. Lahousse, P. Grange, E.M. Gaigneaux, Catalysis Today 117 (2006) 350–355.
[45] C.A. Cellier, V. Vromman, V. Ruaux, E.M. Gaigneaux, P. Grange, Journal of Physical Chemistry B 108 (2004) 9989–10001.
[46] C. Fan, A. Lu, Y. Li, C. Wang, Journal of Colloid and Interface Science 327 (2008) 393–402.
[47] Y.G. Yin, W.Q. Xu, Y.F. Shen, S.L. Suib, C.L. Oyoung, Chemistry of Materials 6 (1994) 1803–1808.
[48] C.D. Wagner, A.V. Naumkin, A. Kraut-Vass, J.W. Allison, C.J. Powell, J.R. Rumble, NIST Standard Reference XPS-Database 20, Version 3.5 (Web Version).
[49] X. Chen, Y.-F. Shen, S.L. Suib, C.L. O'Young, Journal of Catalysis 197 (2001) 292–302.
[50] K. Ramesh, L. Chen, F. Chen, Y. Liu, Z. Wang, Y.-F. Han, Catalysis Today 131 (2008) 477–482.
[51] X.J. Yang, Y.X. Wu, J.Y. Han, H. Yuan, Z.P. Du, Acta Chimica Sinica 67 (2009) 2809–2814.
[52] Z.Y. Pu, X.S. Liu, A.P. Jia, Y.L. Xie, J.Q. Lu, M.F. Luo, Journal of Physical Chemistry C 112 (2008) 15045–15051.
[53] J.L. Ayastuy, M.P. Gonzalez-Marcos, J.R. Gonzalez-Velasco, M.A. Gutierrez-Ortiz, Applied Catalysis B 70 (2007) 532–541.
[54] A. Luengnaruemitchai, D.T.K. Thoa, S. Osuwan, E. Gulari, International Journal of Hydrogen Energy 30 (2005) 981–987.
[55] J. Won Park, J. Hyeok Jeong, W.L. Yoon, C.S. Kim, D.K. Lee, Y.-K. Park, Y.W. Rhee, International Journal of Hydrogen Energy 30 (2005) 209–220.
[56] Q. Guo, Y. Liu, Applied Catalysis B 82 (2008) 19–26.
[57] A. Manasilp, E. Gulari, Applied Catalysis B 37 (2002) 17–25.
[58] S. Funk, B. Hokkanen, E. Johnson, U. Burghaus, Chemical Physics Letters 422 (2006) 461–465.
[59] M.A. Henderson, Surface Science 400 (1998) 203–219.
[60] V.P. Indrakanti, J.D. Kubicki, H.H. Schobert, Fuel Processing Technology 92 (2011) 805–811.
[61] M.A. Henderson, W.S. Epling, C.L. Perkins, C.H.F. Peden, U. Diebold, Journal of Physical Chemistry B 103 (1999) 5328–5337.
[62] R.J.H. Grisel, B.E. Nieuwenhuys, Journal of Catalysis 199 (2001) 48–59.
[63] R.H. Nibbelke, M.A.J. Campman, J.H.B.J. Hoebink, G.B. Marin, Journal of Catalysis 171 (1997) 358–373.
[64] Y.F. Han, M.J. Kahlich, M. Kinne, R.J. Behm, Applied Catalysis B 50 (2004) 209–218.
[65] M.M. Schubert, H.A. Gasteiger, R.J. Behm, Journal of Catalysis 172 (1997) 256–258.
[66] W. Deng, J.D. Jesus, H. Saltsburg, M. Flytzani-Stephanopoulos, Applied Catalysis A 291 (2005) 126–135.
[67] M.M. Schubert, A. Venugopal, M.J. Kahlich, V. Plzak, R.J. Behm, Journal of Catalysis 222 (2004) 32–40.